Velocity-Curvature Relationship of Colliding Spherical Calcium Waves in Rat Cardiac Myocytes

Manfred H. P. Wussling,* Karla Scheufler,* Siegfried Schmerling,# and Volker Drygalla#
*Julius Bernstein Institute of Physiology and #Institute of Numerical Mathematics, Martin Luther University, Halle-Wittenberg, D-06097 Halle, Germany

ABSTRACT Colliding spherical calcium waves in enzymatically isolated rat cardiac myocytes develop new wavefronts propagating perpendicular to the original direction. When investigated by confocal laser scanning microscopy (CLSM), using the fluorescent Ca^{2+} indicator fluo-3 AM, "cusp"-like structures become visible that are favorably approximated by double parabolae. The time-dependent position of the vertices is used to determine propagation velocity and negative curvature of the wavefront in the region of collision. It is evident that negatively curved waves propagate faster than positively curved, single waves. Considering two perfectly equal expanding circular waves, we demonstrated that the collision of calcium waves is due to an autocatalytic process (calcium-induced calcium release), and not to a simple phenomenon of interference. Following the spatiotemporal organization in simpler chemical systems maintained under conditions far from the thermodynamic equilibrium (Belousov-Zhabotinskii reaction), the dependence of the normal velocity on the curvature of the spreading wavefront is given by a linear relation. The so-called velocity-curvature relationship makes clear that the velocity is enhanced by curvature toward the direction of forward propagation and decreased by curvature away from the direction of forward propagation (with an influence of the diffusion coefficient). Experimentally obtained velocity data of both negatively and positively curved calcium waves were approximated by orthogonal weighted regression. The negative slope of the straight line resulted in an effective diffusion coefficient of 1.2×10^{-4} mm^2/s. From the so-called critical radius, which must be exceeded to initiate a traveling calcium wave, a critical volume (with enhanced $[Ca^{2+}]_i$) of ~ 12 μm^3 was calculated. This is almost identical to the volume that is occupied by a single calcium spark.

INTRODUCTION

In solutions with bathing Ca^{2+} of more than 1 mM, single rat cardiac myocytes tend to develop spontaneous calcium waves with different spatiotemporal patterns (Cheng et al., 1996; Lipp and Niggli, 1993; Trafford et al., 1993). It is assumed that a spontaneous calcium wave may originate from a calcium focus, which is composed of a certain but unknown number of Ca^{2+} sparks that are considered to reflect stochastic events of local Ca^{2+} release (Cheng et al., 1993). To determine the critical volume of a so-called hot spot, the investigation of the speed dependence on the curvature of calcium waves proved to be useful. The mechanism of the propagation of those waves is probably determined by the interaction between calcium-induced calcium release (CICR), calcium diffusion, and calcium reuptake (Wier and Blatter, 1991; Williams et al., 1992; Williams, 1993). Cannell et al. (1994) suggested that after release from one or a number of calcium channels of the sarcoplasmic reticulum, a calcium wave propagates faster the smaller the size of the cytosolic volume, into which calcium may diffuse. It was shown, indeed, that 1) the propagation velocity of spherical calcium waves increases with decreasing curvature of the wavefront and 2) calcium, which is released from the sarcoplasmic reticulum, can trigger a spontaneously spreading wave, only when the size of the focus is beyond a critical value (Wussling and Salz, 1996).

Spatiotemporal organization, which is observed in living cells (e.g., calcium waves in cardiac myocytes), also occurs in simpler chemical and biochemical systems maintained under conditions far from thermodynamic equilibrium (Field et al., 1972; Bornmann et al., 1973; Mair and Müller, 1996). One of the most interesting examples of self-organization is the Belousov-Zhabotinskii reaction, which displays temporal oscillations and spatial patterns when malonic acid is catalytically oxidized and brominated by acidic bromate (Field and Burger, 1985; Kuhnert et al., 1985). Depending on the system's excitability, propagating circular waves can develop either spontaneously or must be initiated by a silver wire. The process of wave propagation is mediated by the coupling of an autocatalytic reaction with diffusion. The front of such waves can break up, leading to the generation of open wave ends that can form rotating spiral waves (Keener and Tyson, 1986), a phenomenon that has also been observed in cardiac myocytes (Lipp and Niggli, 1993) and nonmuscle cells (cf. Berridge, 1997). It has been noted previously that there exists a relation between the curvature and the velocity of reaction/diffusion waves (Zykov, 1980; Zykov and Morozova, 1980; Keener, 1986; Keener and Tyson, 1986), which can be approximated by

$$N = c - D * K \quad (1)$$

Received for publication 3 February 1997 and in final form 18 May 1997.
Address reprint requests to Dr. Manfred H. P. Wussling, Julius Bernstein Institute of Physiology, Martin Luther University, Halle-Wittenberg, Magdeburger Strasse 6, D-06097 Halle, Germany. Tel.: 49-345-557-1392; Fax: 49-345-557-4110; E-mail: wussling@medizin.uni-halle.de.

0006-3495/97/09/1232/11 $2.00

where c denotes the velocity of planar waves, D the effective diffusion coefficient, and K the curvature. From Eq. 1 it follows that with increasing curvature the normal velocity either increases or decreases, depending on the sign of the curvature. By definition, positive curvature is the reverse of the radius of outward-propagating circular waves. Negative curvature occurs when two outward-propagating circular waves collide. At the site of collision the sign of the curvature changes. Thus the point of collision always moves fastest until it catches up with the positively curved part of the wave. Equation 1 further predicts a critical radius that must be exceeded to initiate wave propagation ($R_{crit} = 1/K_{crit} = c/D$). Fig. 1 synoptically shows the dependence of the wave speed (N) on both curvature (K, *top*) and radius of expansion (R, *bottom*), where c and D are assumed to be 1. The normalized velocity-curvature relationship results in a straight line (*I*), whereas the velocity-radius relationship yields two branches of a hyperbola (*II*). It is suitable to use the straight line for the determination of R_{crit}, which is obtained by extrapolation to $N = 0$. The upper graph shows that the propagation velocity of the wave front with negative curvature is expected to be higher than that of a positively curved spreading wave. This prediction was experimentally verified by the investigation of colliding circular waves in an excitable medium of the Belousov-Zhabotinskii reaction (Foerster et al., 1988). It also appears that in living cells (e.g., rat cardiac myocytes) the propagation of a wavefront in the region of collision (e.g., of two spherical calcium waves) is faster than the spread of a single circular wave. One goal of this study was to verify this suggestion experimentally in rat cardiac myocytes. Another goal was to determine, by using orthogonal regression of velocity data of both positively and negatively curved calcium wavefronts, the critical radius of a calcium spot and consequently the effective diffusion coefficient.

Because of the cardiac cell's diminutive size, only part of the supposed geometrical form of the wave becomes visible. Extrapolations into the extracellular space proved to be useful for describing the patterns of spreading calcium signals (Girard et al., 1992; Lipp and Niggli, 1993). A certain mathematical effort is required to approximate wavefronts by appropriate functions. These functions are needed for the determination of curvature and velocity in the colliding region of two spherical calcium waves.

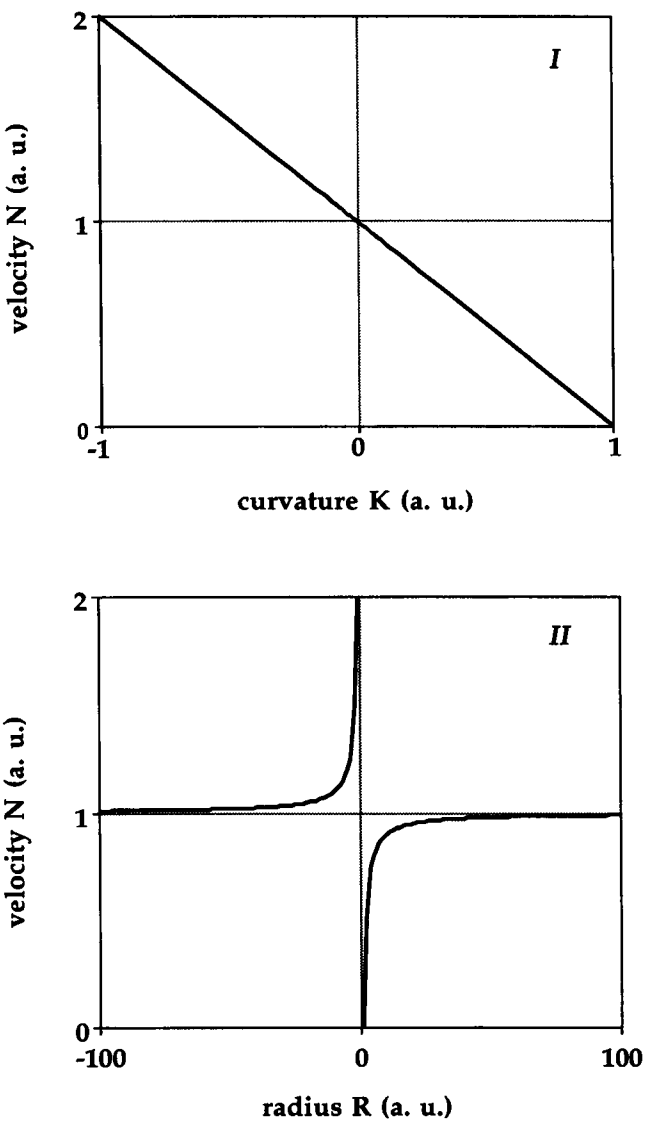

FIGURE 1 Normalized velocity (N)-versus-curvature relationship (straight line, *I*) and velocity-versus-radius relationship (two branches of a hyperbola, *II*). Curves correspond to $N = c - D^*K = c - D/R$, with $c = 1$ and $D = 1$ (a.u., arbitrary units). Curvature K (*upper scale*) as well as radius R (*lower scale*) are negative in the left, and positive in the right part of the corresponding graph. Velocity data of the left parts reflect the propagation of negatively curved wavefronts and are higher than those of positively curved wavefronts (*right parts of the graphs*). The velocity of plane waves corresponds to the point (0, 1). The critical radius below which no wave will propagate is calculated from the intersection of the straight line with the curvature axis and amounts to 1, because of normalization (see *upper graph*). For further explanation see Eq. 1.

METHODS

Preparation and solutions

Rapidly excised hearts of Wistar rats (230–250 g wt) were perfused in a Langendorff apparatus according to a standard procedure. Ventricular cardiocytes were isolated enzymatically and mechanically by stirring small pieces of tissue. Several filtered fractions of isolated cells were stored in HEPES-buffered solution at room temperature. The composition of the solution was (in mM): NaCl 110; KCl 2.6; $CaCl_2$ 1.8; $MgSO_4$ 1.2; KH_2PO_4 1.2; glucose 11; HEPES 25; albumin (Sigma) 1 mg/ml solution; penicillin/streptomycin (10,000 units/10 mg/ml; Biochrom) 0.1 ml/100 ml solution (pH 7.4 at 20°C). Freshly prepared myocytes were loaded with fluo-3 (Molecular Probes, Eugene, OR) by means of a 10-min exposure of 5 μM fluo-3 AM, followed by a 30-min wash to remove the remaining extracellular calcium indicator.

Myocytes with a diastolic sarcomere length of less than 1.8 μm were rejected. The mean sarcomere length (SL) was determined by fast Fourier transform and amounted to 1.86 ± 0.05 μm (mean ± SD, $n = 50$). Myocytes that did not shorten by at least 20% of the mean SL, when electrically stimulated after a 3-min rest, were also omitted (ΔSL: 433 ± 48 nm, mean ± SD, $n = 50$). From cells with spontaneously propagating calcium waves, those with a frequency of less than one per minute at room temperature were selected.

Perfusion chamber and confocal laser scanning microscope

The cell suspension was transferred to the glass bottom of a perfusion chamber (20 mm in diameter and 0.17 mm thickness), which was covered by an identical second plate mounted in a perspex ring. The solution layer's height was 0.5 mm, and the resulting volume was 200 μl. For the measurement of spatiotemporal Ca^{2+} patterns, we used an inverted microscope (Olympus IMT-2) that is part of the confocal laser scanning microscope INSIGHT PLUS (Meridian Instruments, Okemos, MI). The scan system consists of a galvanometer-driven bidirectional mirror (Brakenhoff), which allows image scanning of 512 times 480 pixels, with a speed of 100 scans/s. The speed of image display amounts to 25 scans/s (CCD camera). The light source was an argon ion laser with emission wavelengths of 488 and 514 nm. The Z-drive accessory provides computerized control of optical sectioning with a minimum vertical step of 0.6 μm. Image series showing calcium waves of rat heart cells stained with fluo-3 were saved on a videotape.

Image processing

For the digitization of video frames, we used a frame-grabber board with software package QuickCapture (Data Translation, Marlboro, MA) and a Macintosh Quadra 800 computer. The software used for both the calculation of intensity profiles and object boundaries, as well as for the presentation of images in this paper, was IPLab Spectrum version 3.1 (Signal Analytics, Vienna, VA) and National Institutes of Health Image 1.43 (Microsoft).

RESULTS

Fig. 2 (*top*) shows a fluorescent rat cardiac myocyte with a spontaneous spherical calcium wave, which originated from the outermost right edge. The positive curvature of the spreading wave decreases (compare wavefronts in *a* and *b*). To acquire its position, a strip of the image (20 pixels or 4.5 μm wide) that crosses the wave front perpendicularly was selected as region of interest. At the bottom of Fig. 2, overmodulated profiles of the fluorescence intensity are depicted (*a'*, *b'* correspond to *a*, *b*). The position of the wave front was set, generally, at the maximum step of increasing intensity.

Fig. 3 shows the nonlinear propagating behavior of spherical calcium waves. In Fig. 3 *A*, the time-dependent position of the wavefront of 20 cardiac myocytes is shown ($n = 20$). The experimental conditions were identical ($[Ca^{2+}]$ of the bath solution 1.8 mM, room temperature). At equidistant time points, each data set was locally approximated (see the Appendix). The procedure of nonparametric approximation was repeated with means (see points in Fig. 3 *B*), thus resulting in a curve with an initially small slope that steepens with increasing time. The mean propagation velocity was obtained by differentiation and plotted versus time in Fig. 3 *C*. The oscillations of this curve are not an artifact and may be due to "roughening" by differentiation. Actually, fluctuations of the points in the propagation-time curve (Fig. 3 *B*) are real but too small to become visible here. Fig. 3 *D* shows velocity versus curvature, which is given by the reciprocal of the propagation length. The curve was calculated using simultaneous values of the functions depicted in Fig. 3, *B* and *C*. Again, fluctuations at low curvature reflect the roughening effect of differentiation.

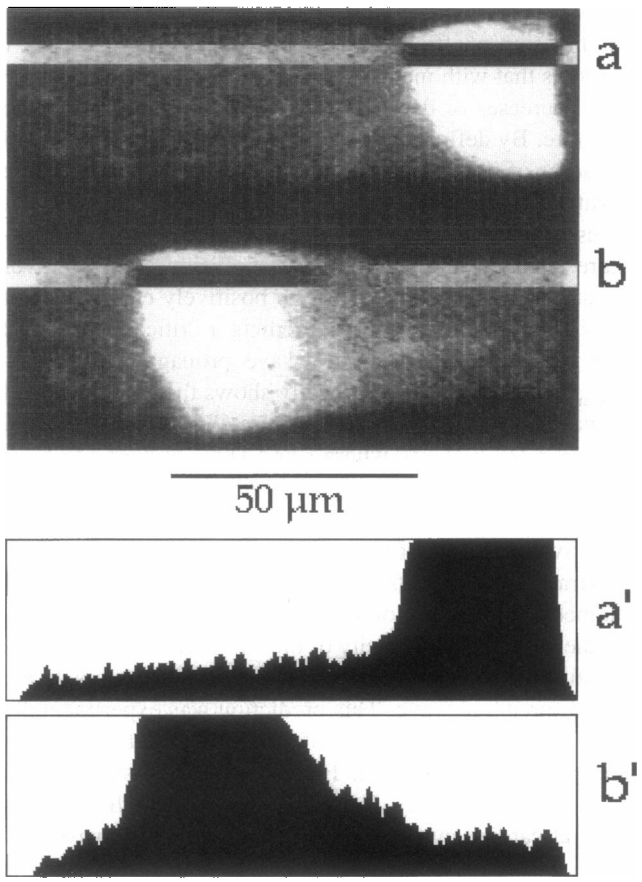

FIGURE 2 Propagation of a spherical calcium wave from the right side to the left side of a rat cardiac myocyte. Cell was loaded with 5 μM fluo-3 AM. (*Top*) A strip of the image is depicted as an inverted region of interest at two different phases of the wave (*a* and *b*). Note: The marked region crosses the wave front perpendicularly. (*Bottom*) Overmodulated intensity profiles of fluorescence were acquired at different moments and positions within the cell (*a'* and *b'*). Position of the wave front was set to where the increasing intensity was at a maximum (see *a'*, *b'*). Identical length calibration for top and bottom.

As mentioned by way of introduction, the curvature of a calcium front appears negative in the region of colliding calcium waves. Subsequently, Fig. 4 shows the development, collision, and annihilation of two spherical calcium waves that appear at different times and places. Selected phases of the calcium signals are indicated by numbers in milliseconds. The actual collision started between 400 and 420 ms, which is shown in the frames of the lower two panels. In the collision zone, "cusp"-like wavefronts develop, drift apart, and reach the side edges of the myocyte. At 480 ms both calcium waves appeared to be practically fused together before the annihilation began. The last frame, at 680 ms, shows a phase of annihilation with two "black holes" placed at two areas with previously enhanced calcium concentration (see frame 400 ms). Fig. 5 *A* shows the fluorescent myocyte at phase 400 ms after rotation by 40°.

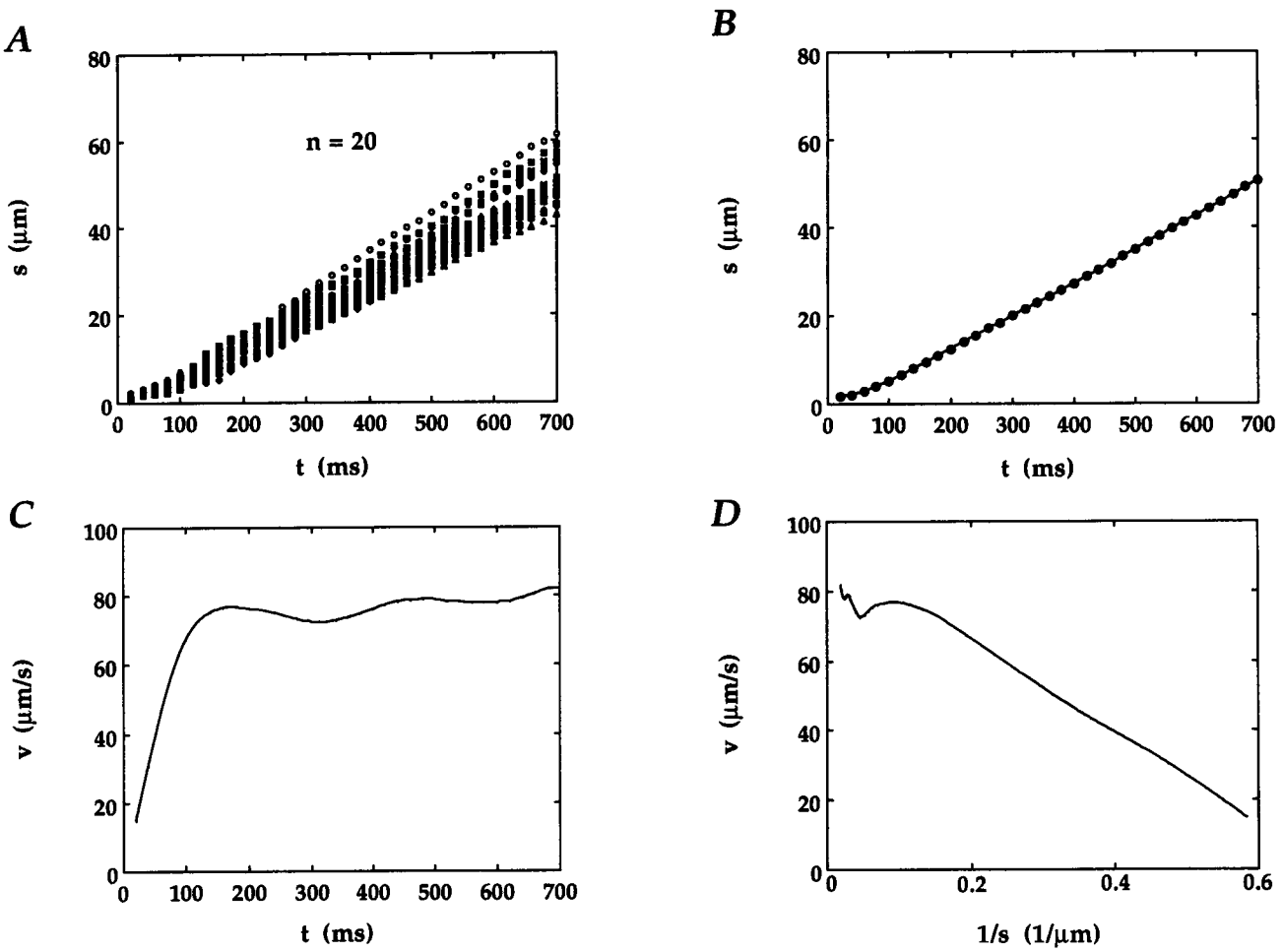

FIGURE 3 Data and analysis of nonlinear propagation of spontaneous spherical calcium waves (s = position of the wave front, t = time, v = ds/dt = propagation velocity, $1/s$ = curvature of the wavefront). (*A*) Data of time-dependent position of spreading waves from 20 different cardiac myocytes. (*B*) Points represent means obtained from the experimental data depicted in *A* by a nonparametric approximation of each data set (n = 20) and subsequent averaging. Nonparametric approximation of the means yields the curve s versus t. (*C*) Propagation velocity versus time as derived from the calculated curve of *B* by differentiation. Oscillations may be due to "roughening" by differentiation. (*D*) Velocity versus curvature was calculated from simultaneous values of the functions depicted in *B* and *C*. Fluctuations at low curvature reflect the "roughening effect" of differentiation.

The corresponding three-dimensional views of the fluorescence intensity in Fig. 5, *B* and *C*, illustrate the determination of the areas of interest. Whereas in Fig. 5 *B* the intensity profile is unfiltered, Fig. 5 *C* shows clusters of fluorescence after normalization with minimum intensity raised from 0 to 128 pixels and maximum intensity remaining at 256 pixels. The boundaries of both of the clusters at the white area define the areas of interest used for the quantitative description of colliding spherical calcium waves. Those areas are shown in Fig. 6 at the start of collision (*a*) and 20 ms thereafter (*b*). Boundaries are not smooth and form more or less wide "cusps" that distinctly drift apart as the collision proceeds.

Fig. 7 illustrates the evaluation of colliding calcium waves. The left panel shows object boundaries that were obtained after enlargement of the areas of interest that are shown in Fig. 6, *a* and *b*, and after sampling by computer. It is important to remark that the "cusps" were approximated by pairs of parabolic functions (see the Appendix for details; the approximation by hyperbolas according to Foerster et al. (1988), who investigated cusplike structures in simpler excitable media of the Belousov-Zhabotinskii reaction, was not satisfying). The overlaid pairs of parabolas differ distinctly from each other after only 20 ms. In the right panel, circles represent experimental data and dotted lines the corresponding approximation curves. The distance of two ticks amounts to 10 pixels or 2.25 μm in both panels. It was an aim of the approximation to quantitatively characterize the propagation of the wave front in the colliding zone. Therefore, we determined the curvature K in the vertices of the parabolae and the half-distance a between them (see *insets* in both parts of the *right panel* of Fig. 7). When observed from that point within a pair of parabolae, which is assumed to be the origin of the new wave after collision, the curves appear convex, so that the curvature is considered to be negative. This is different from the curvature of a spherical wavefront that is concave and positively curved, when observed from the origin of the wave's focus.

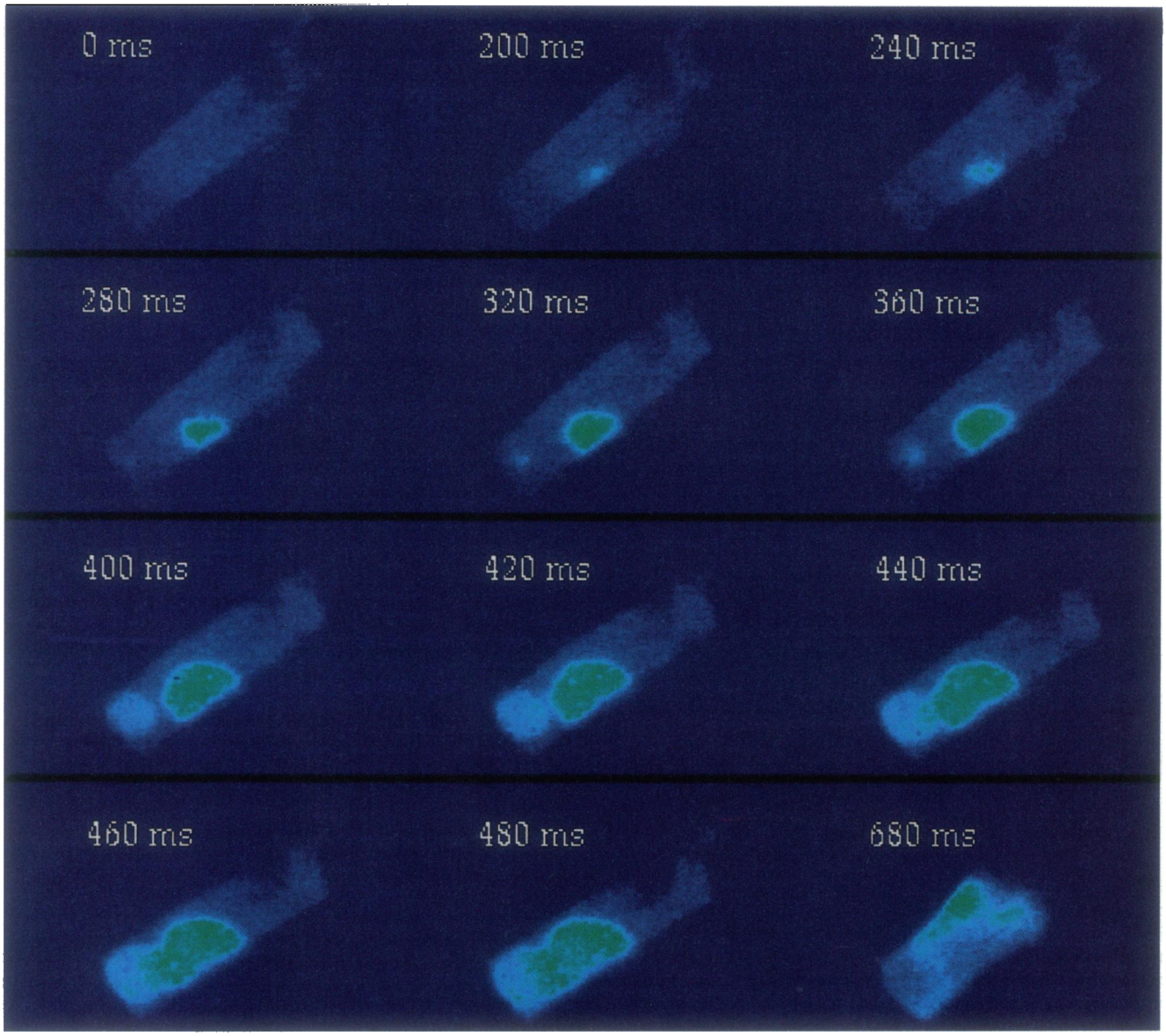

FIGURE 4 Development of the collision of two spontaneous spherical calcium waves in a cardiac myocyte that was loaded with 5 μM fluo 3-AM. Note: The foci develop at different times and positions within the cell. Frames in the lower panels show collisions at several phases. In the last frame (680 ms), the annihilation of the waves becomes visible in the form of two "black holes" in place of two areas with previously enhanced fluorescence intensity (compare to the frame at 400 ms).

Fig. 8 shows a summarizing plot of normal velocity (N) versus curvature (K) of the front of spontaneously propagating calcium waves in rat cardiac myocytes. The squares are based on data resulting from colliding spherical calcium waves as measured in 25 cardiocytes ($n = 25$). It is noticeable that the majority of the velocities are greater at negative than at positive curvature. Circles (means $\pm$ SD) symbolize propagation velocities of single spherical calcium waves, derived from 20 cardiocytes ($n = 20$). The latter data correspond to those of Fig. 3 A, but the circles depicted in Fig. 8 were calculated after averaging of velocity and not propagation length data, both versus time. The advantage of this procedure is explained in the Appendix. All of the data shown in Fig. 8 were approximated by weighted orthogonal regression and resulted in

$$N = 85.7 - 120.1 * K \quad \text{(according to Eq. 1)}$$

with the critical radius $R_{crit} = 1.4$ μm and the diffusion coefficient of $D = 1.2 \times 10^{-4}$ mm^2/s. Plane waves were calculated to spread with a velocity of ~86 μm/s.

DISCUSSION

The results presented in this paper confirm that spherical calcium waves in rat cardiac myocytes propagate in a non-

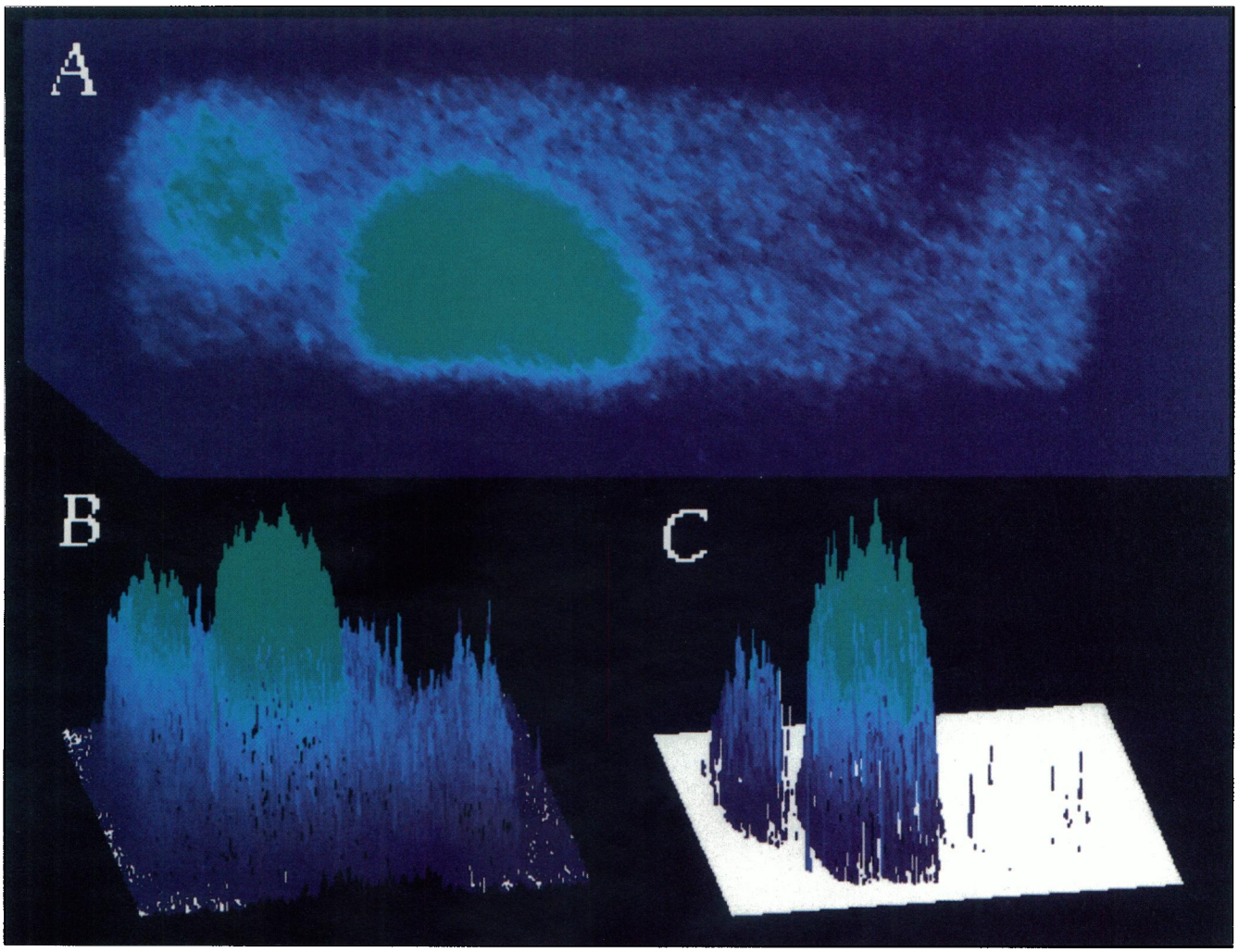

FIGURE 5 Spherical calcium waves immediately before collision and determination of the size of areas of interest. (*A*) The cell corresponds to the frame at 400 ms (Fig. 4) after a rotation of 40°. (*B*) Three-dimensional view of the fluorescence intensity of the whole cell (no subtraction of the background, no filtering). (*C*) Three-dimensional view of the fluorescence intensity of the whole cell after normalization of the intensity (minimum intensity was raised from 0 to 128 pixels, and maximum remained at 256 pixels; linear filtering). Areas of interest are surrounded by the boundaries of both fluorescence clusters.

linear manner with respect to velocity (Wussling and Salz, 1996). Waves with positive curvature start with relatively low velocity and approach a maximum value with increasing radius. When spherical calcium waves collide with each other, they form "cusp"-like fronts that drift apart within a short time. Those wavefronts are considered to be negatively curved. They spread with relatively high velocity from the point of collision and slow down to a minimum value while approaching a planar wavefront. Fig. 8 shows that 1) In general, negatively curved waves propagate faster than those with positive curvature. 2) The normal velocities of negatively and positively curved waves, respectively, aim at the same value at zero curvature, namely 86 μm/s. This is in agreement with previously reported data (Ishide et al., 1990; Williams, 1993; Engel et al., 1995). 3) When fitted by a straight line (according to Eq. 1, describing wave propagation in systems with Belousov-Zhabotinskii reaction), the data yield the critical curvature, where waves do not propagate. From this value, a critical radius of 1.4 μm was calculated, which is on the order of the radius of a calcium spark at half-maximum light intensity (Cheng et al., 1993; Gómez et al., 1996; Lipp and Niggli, 1996; Klein et al., 1996). The corresponding volume with increased $[Ca^{2+}]_i$ amounts to 12 μm^3. It is established that this volume, which must be exceeded to generate a spontaneous calcium wave, practically equals that which is occupied by a single calcium spark (10 μm^3; Cheng et al., 1993). The effective diffusion coefficient of $D = 1.2 \times 10^{-4}$ mm^2/s, resulting from the negative slope of the regression line (cf. Eq. 1 and Fig. 8), corresponds to those of buffered Ca^{2+} in the cytoplasm of various living cells (Lechleiter et al., 1991; Tang and Othmer, 1994; Wang and Thompson, 1995).

During the collision of two calcium waves, a new wavefront develops and propagates perpendicular to the original direction. It is observed that the propagation velocity of the new wavefront is abruptly enhanced immediately after the collision, in comparison to the single wave propagation immediately before the collision. The question that remains

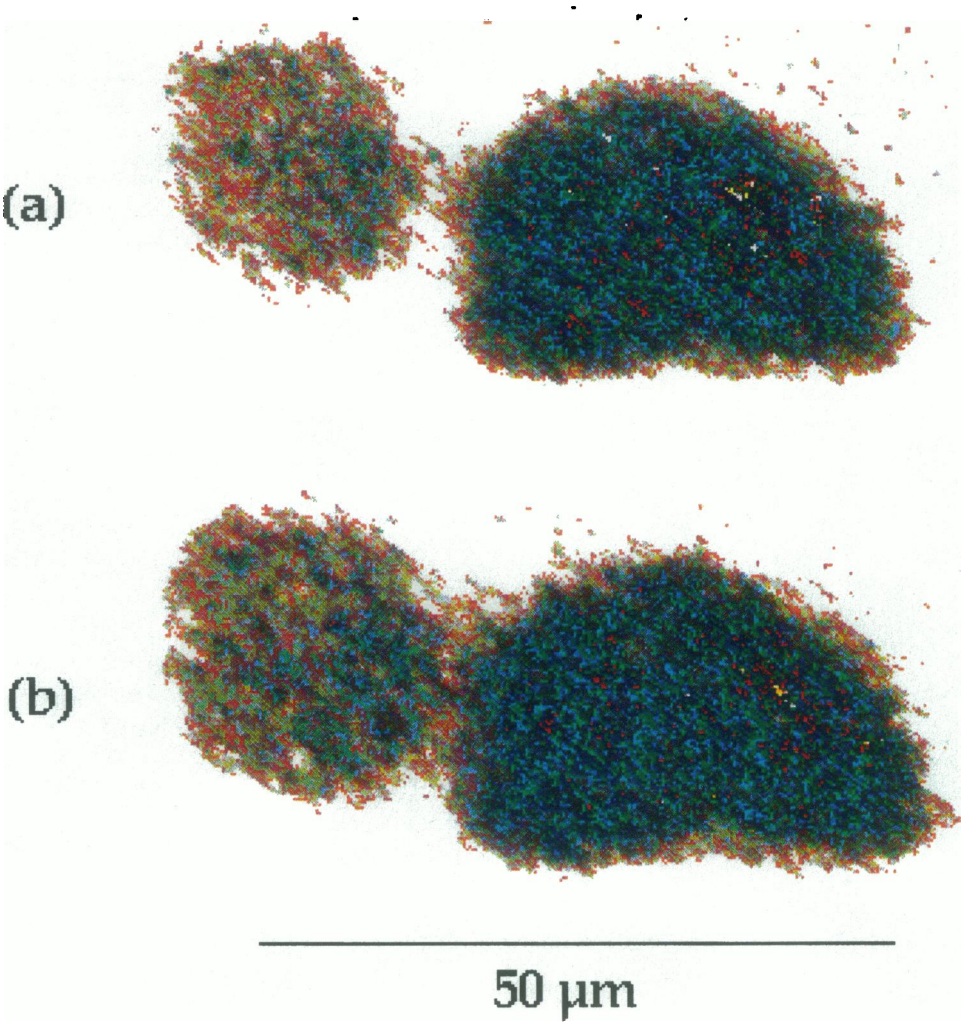

FIGURE 6 Fluorescent areas of interest of two colliding spherical calcium waves. (*a* and *b*) Frames of Fig. 4 at 420 and 440 ms, respectively, each after a rotation and normalization analog to the procedure demonstrated in Fig. 5. Boundaries are unsmooth and develop more or less wide "cusps" that drift apart distinctly within a short time (*b* was obtained 20 ms after *a*).

concerns whether this effect is due to a simple phenomenon of interference. Despite the fact that colliding calcium waves annihilate each other (Ishide et al., 1990), we consider two perfectly equal expanding circular waves that interfere in the physical sense (similar to circular waves on a water surface), with assumed points of intersection at $x = 0$ and $y = \pm\sqrt{(c^2t^2 + 2cr_0t)}$, where t is time, c is the normal speed of a single wave before collision, and r_0 is the radius at $t = 0$ (the moment when the two circles touch each other). The positive velocity of the intersection is given by

$$dy/dt = (c^2t + cr_0)/y \qquad (2)$$

To better compare the physical phenomenon of interfering surface waves to the phenomenon of colliding calcium waves, Fig. 9 shows the velocity of the wavefront, dy/dt, during interference and collision, respectively, versus the reciprocal of its position, $1/y$. Fig. 9, curve *a*, corresponds to the physical phenomenon of interference of two circular waves and is calculated from Eq. 2, with the assumptions of $c = 86$ μm/s (see Fig. 8, velocity of plane calcium waves according to the intersection of the straight line with the velocity axis) and $r_0 = 86$ μm. Fig. 9, curve *b*, shows the regression line of experimentally obtained data from colliding calcium waves, where $1/y$ represents the reciprocal of the half-distance between the vertices of parabolae (cf. Fig. 7, *right*). It should be mentioned that squares in Fig. 9 correspond to, but are not identical to, the curvature-related squares in Fig. 8. The slope of curve *b* in Fig. 9, however, is clearly different from that of curve *a*, thus suggesting that the enhancement of the propagation velocity (immediately after the collision of calcium waves) and its succeeding decrease are due to an autocatalytic process rather than a simple phenomenon of interfering circular waves.

During the collision, both single waves are expected to undergo a deformation of the wavefronts in the colliding region. This implication results from the observation that the common wavefront propagates with enhanced velocity, although it was slower than predicted from Eq. 2. In other words, the propagation velocity of single waves is slowed down during collision and subsequent annihilation. A possible explanation is the mutual hindrance of the diffusion of Ca^{2+} that was released from the sarcoplasmic reticulum.

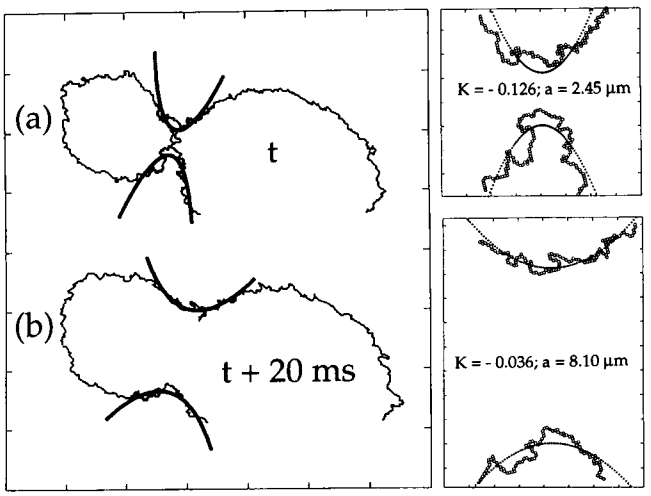

FIGURE 7 Illustration of the evaluation of colliding calcium waves. (*Left*) Areas of interest are surrounded by lines, both after normalization of fluorescence intensity (Fig. 5), and agree with the areas of Fig. 6. The "cusps" were approximated in pairs by parabolic functions, and the corresponding curves, which differ from each other, are overlayed. (*Right*) The upper part of the panel corresponds to *a*, and the lower part corresponds to *b*. Circles represent experimental data. They are given by the values of abscissa, ordinate, and intensity after the computerized determination of the "cusp" boundaries. The division at the axes is 10 pixels ($\approx$ 2.25 μm) in both panels. The procedure of approximation by parabolae (*dotted lines*) is described in the Appendix. *K* represents the curvature at the vertex of a parabola (in 1/μm) and is considered to be negative (see text for explanation). *a* is the half-distance between the vertices of the corresponding parabolae (in μm). *t* represents time (*left*). Note the changes in *K* and *a* from top to bottom (i.e., within 20 ms).

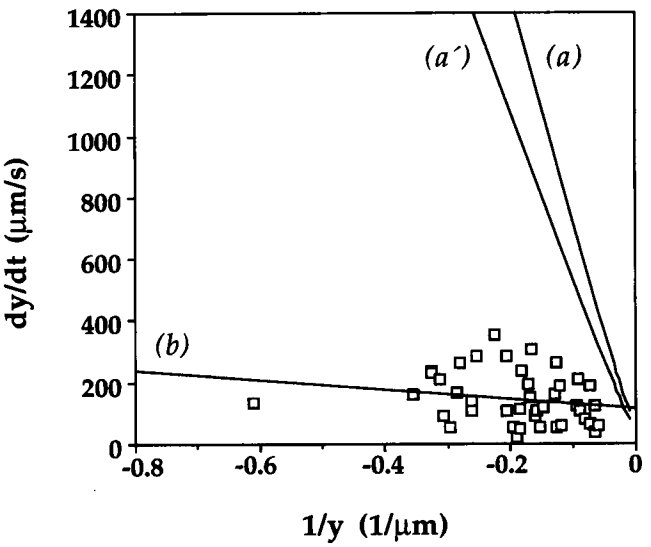

FIGURE 9 (*a*) Velocity of the intersection of two expanding and interfering circular waves versus the reciprocal of the distance between the point of touching at $t = 0$ (see text) and the intersection at any given moment. (*a'*) Data obtained after division of curve *a* by 1.36 (see text for explanation). (*b*) Velocity of the "cusps" of two propagating and colliding spherical calcium waves versus the reciprocal of the half-distance between the vertices of the parabolae, used for the approximation of the "cusps."

This is caused by increased cytosolic $[Ca^{2+}]_i$ in the region of collision, thus acting as a diffusion barrier in the direction of the single-wave propagation immediately before collision. Unfortunately, because of a certain inhomogeneity of the fluorescent light signals and the relatively small size of cardiac myocytes, the expected collision-induced deformation of the single wavefront would be nearly impossible to resolve.

It has been shown that calcium waves in cardiac myocytes propagate faster in the longitudinal than in the transverse direction (Engel et al., 1994; Parker et al., 1996). In our experiments, we observed negatively curved wavefronts (i.e., those after collision) traveling mainly in the transverse direction of the cell. Therefore it was necessary to take into account that diffusion within cardiac myocytes is anisotropic. Considering the enhanced but unreduced velocities of negatively curved in comparison to positively curved calcium waves (see Fig. 8), an essential influence of the reduction of the propagation velocity by traveling in a transverse direction can be excluded. Furthermore, we have divided the data of curve *a* in Fig. 9 by 1.36 (mean ratio of

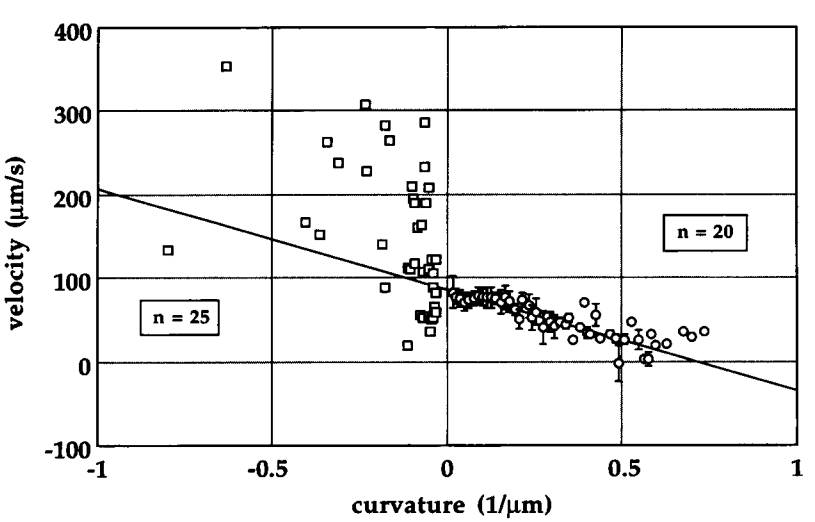

FIGURE 8 Normal velocity (*N*) versus curvature (*K*). □, Data resulting from colliding spherical calcium waves acquired from 25 cardiac cells ($n = 25$). ○, Spherical calcium waves (means ± SD) ($n = 20$, data shown in Fig. 3 *A*). The data were approximated by orthogonal weighted regression (see Appendix) and resulted in $N = 85.7 - 120.1*K$ (according to Eq. 1: $N = c - D*K$), with the critical radius $R_{crit} = 1.4$ μm and the effective diffusion coefficient $D = 1.2 \times 10^{-4}$ mm^2/s.

velocities longitudinal/transverse; Engel et al., 1994) and obtained curve a'. Even if we consider a certain effect of anisotropy on the propagation velocity of circular waves, there remains a discrepancy between the model of interference (Fig. 9, curves a and a') and colliding calcium waves in cardiac myocytes (Fig. 9, curve b). Obviously, the velocity-curvature relationship (Eq. 1) is most suitable for the description of spontaneous calcium waves in living cells.

In summary, colliding calcium waves develop "cusp"-like, negatively curved fronts that propagate considerably faster than single waves. Collision-induced velocity enhancement is not due to interference; rather it obeys the velocity-curvature relationship derived from chemical systems with autocatalytic properties (Belousov-Zhabotinskii reaction). Supposedly, the spatiotemporal patterns of both negatively and positively curved calcium waves essentially depend on the effective diffusion coefficient of cytosolic Ca^{2+}. A critical volume with enhanced $[Ca^{2+}]_i$ on the order of a single calcium spark is suggested to initiate the propagation of traveling calcium waves.

APPENDIX

Remarks on mathematical handling for single waves

Single spherical calcium waves were observed in 20 cells. The measured values s_{ij}, $i = 1, \ldots, 20$, $j = 1, \ldots, 35$, of the way at the time points $t_j = 0.02 \cdot j$ can be modeled by

$$s_{ij} = s_i(t_j) + e_{ij} \tag{A1.1}$$

where the unknown functions $s_i(t)$ are supposed elements of a Sobolev room $W_2^6(-\infty, +\infty)$ and the unknown e_{ij} are supposed realizations of random errors.

The substitution of $s_i(t)$ in the models (A1.1) by truncated Taylor expansions,

$$s_i(t_0 + (t - t_0)) \approx s_i(t_0) + (t - t_0) \cdot s_i^{(1)}(t_0) + \cdots + \frac{(t - t_0)^5}{5!} \cdot s_i^{(5)}(t_0)$$

and introduction of Gaussian weight functions,

$$w_{ij}(t_0; t_j, h) := \exp\left\{-\frac{1}{2}\frac{(t_j - t_0)^2}{h^2}\right\}$$

with a smoothing parameter $h > 0$ results in so-called local models,

$$s_{ij} = s_i(t_0) + (t_j - t_0) \cdot s_i^{(1)}(t_0) + \cdots + \frac{(t_j - t_0)^5}{5!} \cdot s_i^{(5)}(t_0) + \frac{e_{ij}}{\sqrt{w_{ij}}} \tag{A1.2}$$

for each i and for each fixed t_0 from $[t_1; t_{35}]$.

By least squares,

$$Q_i := \sum_{j=1}^{35} w_{ij}(t_0; t_j, h) \cdot \left\{s_{ij} - s_i(t_0) - (t_j - t_0)s_i^{(1)}(t_0) - \cdots - \frac{(t_j - t_0)^5}{5!} s_i^{(5)}(t_0)\right\}^2 \to \min \tag{A1.3}$$

one can obtain both smoothed values $\hat{s}_i(t_0)$ of the way $s_i(t_0)$ and smoothed values $\hat{s}_i^{(1)}(t_0)$ of the velocity $s_i^{(1)}(t_0)$ for each time point t_0 (Schmerling and Peil, 1989).

In this manner we found from (A1.3), with $h = 0.08$, velocity estimates $\hat{v}_{ij} := \hat{s}_i^{(1)}(t_j)$ for $i = 1, \ldots, 20$ and $j = 1, \ldots, 35$. The mean values $\bar{v}_j$ for all cells

$$\bar{v}_j = \frac{1}{20}\sum_{i=1}^{20} \hat{v}_{ij}$$

at the time points t_j are demonstrated as a curve in Fig. 3 *C*.

The sample variances

$$vs_j^2 := \frac{1}{20}\sum_{i=1}^{20}(\hat{v}_{ij} - \bar{v}_j)^2$$

are needed as accuracies in the following weighted orthogonal regression.

Weighted orthogonal regression

There are given velocity mean values $\bar{v}_l$ with their sample variances vs_l^2 and curvature mean values $\bar{k}_l$ with their sample variances ks_l^2.

Between the true values v_l° and k_l°, a linear functional relationship

$$v_l^\circ = \alpha + \beta \cdot k_l^\circ$$

for $l = 1, \ldots, n$ is assumed.

According to Sprent (1969), we must estimate α and β from

$$Q^* := \sum_{l=1}^{n} \frac{(\bar{v}_l - \alpha - \beta \cdot k_l^\circ)^2}{vs_l^2} + \sum_{l=1}^{n} \frac{(\bar{k}_l - k_l^\circ)^2}{ks_l^2} \to \min \tag{A2.1}$$

which is equivalent to

$$Q^\circ = \sum_{l=1}^{n} \frac{(\bar{v}_l - \alpha - \beta \cdot \bar{k}_l)^2}{vs_l^2 + \beta^2 \cdot ks_l^2} \to \min \tag{A2.2}$$

(weighted orthogonal regression). From (A2.2) we found estimates $\hat{\alpha}$ and $\hat{\beta}$ by Gauss-Newton iteration. The result of this evaluation is demonstrated as a straight line in Fig. 8.

Fitting data by a double parabola

In the area of collision, the "cusps" were approximated by a double parabola. It can be described by the parametric representation

$$x = x_0 + (p - x_0)\cos\phi - (a + b(p - x_0)^2)\sin\phi$$
$$y = y_0 + (p - x_0)\sin\phi + (a + b(p - x_0)^2)\cos\phi$$
$$p \in (-\infty, \infty)\text{(upper part)}$$

and

$$x = x_0 + (p - x_0)\cos\phi + (a + b(p - x_0)^2)\sin\phi$$
$$y = y_0 + (p - x_0)\sin\phi - (a + b(p - x_0)^2)\cos\phi$$
$$p \in (-\infty, \infty)\text{(lower part)}$$

(x_0, y_0) is the center of the parabola, a the distance from the center to the vertex, and ϕ the (small) angle of rotation. The curvature becomes $-2b$.

Every point (ξ_i, η_i) of the boundary of the "cusps" is approximated by a point (x_i, y_i) of the parabola, i.e., we must find parameters $p_1, \ldots, p_n, x_0, y_0, a, b, \phi$ such that

$$\|F(p_1, \ldots, p_n, x_0, y_0, a, b, \phi)\|_2^2 \rightarrow \min$$

where

$$F(.) = \begin{pmatrix} \xi_1 - x_0 - (p_1 - x_0)\cos\phi + sign(\eta_1 - y_0)(a + b(p_1 - x_0)^2)\sin\phi \\ \cdots \\ \xi_n - x_0 - (p_n - x_0)\cos\phi + sign(\eta_n - y_0)(a + b(p_n - x_0)^2)\sin\phi \\ \eta_1 - y_0 - (p_1 - x_0)\sin\phi - sign(\eta_1 - y_0)(a + b(p_1 - x_0)^2)\cos\phi \\ \cdots \\ \eta_n - y_0 - (p_n - x_0)\sin\phi - sign(\eta_n - y_0)(a + b(p_n - x_0)^2)\cos\phi \end{pmatrix}$$

The points (ξ_i, η_i) are well separated into an upper and a lower area, respectively (i.e., even though the determination of y_0 is part of the minimization process, the values of $\text{sign}(\eta_i - y_0)$ do not change throughout the computation, if the initial values are chosen properly).

The problem is solved by Gauss-Newton iteration (cf. Fletcher, 1987). Note that the Jacobian has the form

$$J = \begin{pmatrix} D_1 & A \\ D_2 & B \end{pmatrix},$$

where D_1 and D_2 are diagonal and A and B are $n \times 5$-blocks. That is, the computation of $(J^TJ)^{-1}J^TF$—what must be done in every Gauss-Newton step—can be organized in such a way that it requires $\mathcal{O}(n)$ floating point operations only.

We thank Dr. Th. Mair for stimulating and helpful discussions, S. Boldt and C. Girke for technical assistance, and M. Paetzel for helping us with the manuscript.

This work was supported by the Deutsche Forschungsgemeinschaft.

REFERENCES

Berridge, M. J. 1997. Annual Review Prize Lecture: elementary and global aspects of calcium signalling. *J. Physiol. (Lond.).* 499.2:291–306.

Bornmann, L., H. Busse, and B. Hess. 1973. Oscillatory oxidation of malonic acid by bromate. *Z. Naturforsch.* 28 c:514–516.

Cannell, M. B., H. Cheng, and W. J. Lederer. 1994. Spatial non-uniformities in $[Ca^{2+}]_i$ during excitation-contraction coupling in cardiac myocytes. *Biophys. J.* 67:1942–1956.

Cheng, H., W. J. Lederer, and M. B. Cannell. 1993. Calcium sparks—elementary events underlying excitation-contraction coupling in heart muscle. *Science.* 262:740–744.

Cheng, H., M. R. Lederer, W. J. Lederer, and M. B. Cannell. 1996. Calcium sparks and $[Ca^{2+}]_i$ waves in cardiac myocytes. *Am. J. Physiol. (Cell Physiol.* 39):C148–C159.

Engel, J., M. Fechner, A. J. Sowerby, S. A. E. Finch, and A. Stier. 1994. Anisotropic propagation of Ca^{2+} waves in isolated cardiomyocytes. *Biophys. J.* 66:1756–1762.

Engel, J., A. J. Sowerby, S. A. E. Finch, M. Fechner, and A. Stier. 1995. Temperature dependence of the mechanism of autocatalytic Ca^{2+} release in wave propagation. *Biophys. J.* 68:40–45.

Field, R. J. and M. Burger. 1985. Oscillations and Traveling Waves in Chemical Systems. Wiley, New York.

Field, R. J., E. Körös, and R. M. Noyes. 1972. Oscillations in chemical systems. II. Thorough analysis of temporal oscillations in the bromate-cerium-malonic acid system. *J. Am. Chem. Soc.* 94:8649–8664.

Fletcher, R. 1987. Practical Methods of Optimization, 2nd Ed. Wiley, Chicester, England.

Foerster, P., S. C. Müller, and B. Hess. 1988. Curvature and propagation of chemical waves. *Science.* 241:685–687.

Foerster, P., S. C. Müller, and B. Hess. 1989. Critical size and curvature of wave formation in an excitable chemical medium. *Proc. Natl. Acad. Sci. USA.* 86:6831–6834.

Girard, S., A. Lückhoff, J. Lechleiter, J. Sneyd, and D. Clapham. 1992. Two-dimensional model of calcium waves reproduces the patterns observed in *Xenopus* oocytes. *Biophys. J.* 61:509–517.

Gómez, A. M., H. Cheng, W. J. Lederer, and D. M. Bers. 1996. Ca^{2+} diffusion and sarcoplasmic reticulum transport both contribute to $[Ca^{2+}]_i$ during Ca^{2+} sparks in rat ventricular myocytes. *J. Physiol. (Lond.).* 496.2:575–581.

Ishide, N., T. Urayama, K. I. Inoue, T. Komaru, and T. Takishima. 1990. Propagation and collision characteristics of calcium waves in rat myocytes. *Am. J. Physiol.* 259 (*Heart Circ. Physiol.* 28):H940–H950.

Keener, J. P. 1986. A geometrical theory for spiral waves in excitable media. *SIAM J. Appl. Math.* 46:1039–1056.

Keener, J. P. and J. J. Tyson. 1986. Spiral waves in the Belousov-Zhabotinskii reaction. *Physica.* 21D:307–324.

Klein, M. G., H. Cheng, L. F. Santana, Y.-J. Jiang, W. J. Lederer, and M. F. Schneider. 1996. Two mechanisms of quantized calcium release in skeletal muscle. *Nature.* 379:455–458.

Kuhnert, L., H.-J. Krug, and L. Pohlmann. 1985. Velocity of trigger waves and temperature dependence of autowave processes in the Belousov-Zhabotinskii reaction. *J. Phys. Chem.* 89:2022–2026.

Lechleiter, J., S. Girard, E. Peralta, and D. Clapham. 1991. Spiral calcium wave propagation and annihilation in *Xenopus laevis* oocytes. *Science.* 253:123–126.

Lipp, P., and E. Niggli. 1993. Microscopic spiral waves reveal positive feedback in subcellular calcium signaling. *Biophys. J.* 65:2272–2276.

Lipp, P., and E. Niggli. 1996. Submicroscopic calcium signals as fundamental events of excitation-contraction coupling in guinea-pig cardiac myocytes. *J. Physiol. (Lond.).* 492.1:31–38.

Mair, T., and S. C. Müller. 1996. Traveling NADH and proton waves during oscillatory glycolysis in vitro. *J. Biol. Chem.* 271:627–630.

Parker, I., W.-J. Zang, and W. G. Wier. 1996. Ca^{2+} sparks involving multiple Ca^{2+} release sites along Z-lines in rat heart cells. *J. Physiol. (Lond.).* 497.1:31–38.

Schmerling, S., and J. Peil. 1989. Local approximations and its applications in statistics. *Gegenbaurs Morphol. Jahrb.* 135:255–260.

Sprent, P. 1969. Models in Regression and Related Topics. Methuen, London.

Tang, Y., and H. G. Othmer. 1994. A model of calcium dynamics in cardiac myocytes based on the kinetics of ryanodine-sensitive calcium channels. *Biophys. J.* 67:2223–2235.

Trafford, A. W., S. C. O'Neill, and D. A. Eisner. 1993. Factors affecting the propagation of locally activated systolic Ca transients in rat ventricular myocytes. *Pflügers Arch.* 425:181–183.

Wang, S. S.-H., and S. H. Thompson. 1995. Local positive feedback by calcium in the propagation of intracellular calcium waves. *Biophys. J.* 69:1683–1697.

Wier, W. G., and L. A. Blatter. 1991. Ca^{2+} oscillations and Ca^{2+} waves in mammalian cardiac and vascular smooth muscle cells. *Cell Calcium.* 12:241–254.

Williams, D. A. 1993. Mechanism of calcium release and propagation in cardiac cells. Do studies with confocal microscopy add to our understanding? *Cell Calcium.* 14:724–735.

Williams, D. A., L. M. Delbridge, S. H. Cody, P. J. Harris, and T. O. Morgan. 1992. Spontaneous and propagated calcium release in isolated cardiac myocytes viewed by confocal microscopy. *Am. J. Physiol.* 262 (*Cell Physiol.* 31):C731–C742.

Wussling, M. H. P., and H. Salz. 1996. Nonlinear propagation of spherical calcium waves in rat cardiac myocytes. *Biophys. J.* 70:1144–1153.

Zykov, V. S. 1980. Analytical evaluation of the dependence of the speed of an excitation wave in two-dimensional excitable medium on the curvature of its front. *Biophysics.* 25:906–1011.

Zykov, V. S., and O. L. Morozova. 1980. Biophysics of complex systems. Speed of spread of excitation in a two-dimensional excitable medium. *Biophysics.* 24:739–744.